

Finite size effects in active microrheology in colloids

F. Orts^a, G. Ortega^b, E.M. Garzón^a, A.M. Puertas^{c,*}

^a*Supercomputation-Algorithms Group, Dpt. of Informatics, Univ. of Almería, ceiA3, Ctra. Sacramento s/n, 04120, Almería, Spain*

^b*Computer Architecture Dpt., Universidad de Málaga, E.T.S.I. Informática Campus Teatinos, 29071, Málaga, Spain*

^c*Group of Complex Fluids Physics, Dpt. of Applied Physics, Univ. of Almería, Ctra. Sacramento s/n, 04120, Almería, Spain*

Abstract

Active microrheology has emerged in recent years as a new technique to probe microscopically the mechanical properties of materials, particularly, viscoelastic ones. In this technique, a colloidal tracer is pulled through the material, and its dynamics is monitored. The interpretation of results usually relies on the Stokes-Einstein approximation, which is valid for a continuous medium in equilibrium. In this work, we have studied with simulations a suspension of quasi-hard colloidal spheres, where a large tracer is pulled by a constant force. The Navier-Stokes equation for a continuous bath predicts important finite size effects, decaying as the inverse box size, which require simulations of different systems to extract the microviscosity of a bulk system. A strategy to optimize the scheduling of the simulation tasks on a multi GPU-CPU cluster based on the adaptation of a genetic algorithm is presented here, and used to study the effect of different conditions on the friction experienced by the tracer (adding the tracer volume to the total system volume, fixing the center of mass of the system, varying the fluid friction coefficient and tracer size). It is observed that the theoretical prediction is not followed, but deviations are observed for large systems in all cases. These are attributed to the finite size of the bath particles, and the intrinsic dynamics of colloidal systems, as shown by the analysis of the velocity profile in the bath.

Keywords: Microrheology, Finite size effects, Scheduling in CPU-GPU clusters, Simulations of colloids

*Corresponding author

Email address: apuertas@ual.es (A.M. Puertas)

1. Introduction

Soft matter is characterized by the interplay of very different length and time scales. Physically, this is achieved, e.g., in suspensions of macromolecules or colloids, where the solvent degrees of freedom and macromolecule diffusion extend over many different scales [1, 2]. This poses a major problem in resolving all of them, both computationally and experimentally, which is typically tackled integrating out the fast degrees of freedom, or using effective models [3]. The canonical example is probably Brownian hard spheres, where internal degrees of freedom are absent and the solvent dynamics is integrated in the so-called Brownian motion; still, the separation between short time and long time diffusion of the colloidal particles provokes viscoelastic behavior when the glass transition is approached.

In order to probe the complex mechanical behaviour of soft matter, several techniques have been developed [4]. In addition to the direct measurement using bulk rheology, where macroscopic stresses are applied, microrheology has emerged over the last decades as a new methodology, both in the passive or active modes [5, 6, 7, 8]. Here, the dynamics of a tracer (typically of colloidal size) is studied, with an external force driving it (active microrheology), or without any force (passive microrheology). This approach, initially thought for expensive or difficult to obtain samples [9, 10], but still in development [11, 12], requires a deep understanding of the interplay of the dynamics of bath and tracer, in particular due to the non-affine strain field provoked by the latter [13, 14]. It is therefore compulsory to test the theory models to be used in the interpretation of the results.

Computer simulations have emerged as an ideal tool to test these models, using simple systems, whose bulk properties are well-known [7]. However, because simulations consider always a finite number of particles, finite-size effects can appear. This is even more plausible, since the hydrodynamic correlations, expected from models based on a continuum description of the bath [15], have a very long range. This makes the simulation work a formidable task because a large number of particles have to be considered to obtain the trajectory of a single tracer; even more, a large number of trajectories are needed to average out the thermal noise and initial conditions; and finally different system sizes have to be considered [16, 17].

Previous simulation works in this line have focused on passive microrhe-

ology, i.e. the dynamics of a large unperturbed tracer, in a bath of hard spheres undergoing Newtonian dynamics [16, 17, 18, 19, 20]. In this way, those works have simulated the motion of a nanocolloidal particle, resulting in Brownian motion, and the fluctuation-dissipation theorem. The results show good qualitative agreement with the predictions from continuum theory for the bath, and when the tracer is larger than around five times the bath particles the agreement is quantitative. Active microrheology in a bath of hard spheres, on the other hand, has been studied with tracers of size comparable to the bath particles, with Brownian, Langevin, or Stokesian microscopic dynamics [7, 21, 22, 23, 24, 25, 26, 28]. Both the simulation and theoretical models show that the effective friction coefficient experienced by the tracer has a plateau for small pulling forces, where the properties of the bath are probed – linear response and generalized Stokes-Einstein relations are expected to be applicable here. Upon increasing the driving force, the effective friction enters a so-called force-thinning regime, where the coefficient decreases, until a plateau is eventually reached for strong pullings [29].

We present here simulations of active microrheology in a system of quasi-hard Brownian spheres with large tracers. These, however, are affected by strong finite size effects, requiring simulations of different sizes. Given the large number of independent simulations of different lengths, a multi GPU-CPU cluster was used, which supplies processors with several CPU-cores and GPUs. A sequential code to compute simulations on CPU-cores, and a parallelized one for computing on GPUs, prepared previously [30], have been used. To reduce the runtime for the set of simulations it is very important to distribute the different simulations among CPU-cores and GPUs in a balanced way, i.e. with a minimal idle processors time. This is a challenge due to the heterogeneity of simulations and computational power of CPU-cores and GPUs. A genetic algorithm has been implemented to obtain a near optimal balance in the distribution of simulations on the clusters, which is the result of this work (freely available at <https://github.com/2forts/GENS>). We focus on a system with a bath volume fraction of 50%, and a tracer three times larger than the bath particles. The scheme presented here optimizes the whole set of simulations required to analyze the friction coefficient. The acceleration of the single trajectories, due to the GPU parallelization, has allowed us to simulate large systems and study the effects of different parameters of the simulations of active microrheology in colloidal hard spheres, aiming to identify the optimal simulation conditions to test the theoretical model. For large systems, the simulation data deviate from the theoretical

prediction, and the velocity field in the bath oscillates in phase with the density. More interestingly, we show that the velocity in the bath decays faster than predicted, and becomes negligible for distances similar to the simulation box size where the deviations appear.

The manuscript is organized as follows: In Section 2 the physical system is described, and the model used for its analysis introduced. Our scheme for the distribution of the tasks among the computational resources is described in section 3. Section 4 is devoted to the presentation of the results, in particular analysing the effects of the consideration of the volume of the tracer, the size of the tracer, or fixing the center of mass of the systems. In the final part of this section, we study the velocity profile induced in the bath by the moving tracer, and compare it with the theoretical predictions from the Navier-Stokes equation. Finally, the conclusions are presented in Section 5.

2. System details

Microrheology in a colloidal system is simulated considering N polydisperse Brownian particles containing the tracer (labeled with $j = 1$) in a cubic box with periodic boundary conditions. Microscopic Brownian dynamics is modelled with the Langevin equation of motion, which for particle j reads [35]:

$$m_j \frac{d^2 \mathbf{r}_j}{dt^2} = \sum_{i \neq j} \mathbf{F}_{ij} - \gamma_j \frac{d \mathbf{r}_j}{dt} + \mathbf{f}_j(t) + \mathbf{F}_{ext} \delta_{j1} \quad (1)$$

where m_j is the particle mass, and the terms in the right hand side correspond to the interaction forces between particles i and j , the friction with solvent, Brownian force and the external force, which acts only on the tracer (as shown by the Kronecker-delta symbol, δ_{j1}). The friction force is proportional to the particle velocity, and the proportionality constant is given by $\gamma_i = \gamma_0 a_i$, where a_i is the particle radius. This expression mimics the Stokes formula for low Reynolds numbers, $\gamma_i = 6\pi\eta a_i$, where η is the solvent viscosity. The Brownian force, $\mathbf{f}(t)$, is random, but its intensity is linked to the friction force, as given by the fluctuation-dissipation theorem, $\langle \mathbf{f}_j(t) \cdot \mathbf{f}_j(t') \rangle = 6k_B T \gamma_j \delta(t - t')$, where $k_B T$ is the thermal energy and $\delta(x)$ is the Dirac-delta symbol [35].

The direct interaction between particles i and j is derived from the central inverse-power potential:

$$V(\mathbf{r}) = k_{\text{B}}T \left(\frac{r}{a_{ij}} \right)^{-36} \quad (2)$$

with $r = |\mathbf{r}|$ and a_{ij} the center to center distance between the particles. It has been shown previously that with this potential the particles behave effectively as hard spheres [36]. To avoid crystallization at high density, size polydispersity is introduced in the bath. Sizes for the bath particles are selected from a flat distribution of width $2\delta = 0.2a$, with a the mean radius of the bath particles. All particles, including the tracer, have the same mass: $m_j = m$.

In the simulations, the system is equilibrated with the tracer for a long time without the external force. At $t = 0$, the external force is switched on, and the tracer trajectory is recorded. The long-time steady tracer velocity, $\langle v \rangle$, is calculated as the slope of the tracer displacement vs. time, and averaged over many independent trajectories. This allows the calculation of the effective friction coefficient using the steady-state relationship $F_{\text{ext}} = \gamma_{\text{eff}} \langle v \rangle$. Previous simulations (with tracers of the same size as the bath particles) have shown that γ_{eff} develops a plateau for small forces, indicating a linear regime (Newtonian behaviour) [7, 21, 22]. We intend to focus here in this linear regime for small forces, using tracers larger than the bath particles.

However, the use of periodic boundary conditions in the three dimensions implies that the actual simulated system is a cubic array of tracers pulled in an infinite bath. Because the lattice spacing in this array of tracers is given by the size of the simulation box, this is a finite size effect. In order to analyze, and eventually correct it, a continuum model based on solving the Navier-Stokes equation for an infinite array of tracers in a Newtonian viscous fluid is used [15]. Hasimoto [15] showed that the friction coefficient, γ_{eff} , experienced by a cubic array of tracers is related to the lattice spacing, L , as:

$$\frac{1}{\gamma_{\text{eff}}} = \frac{1}{\gamma_{\infty}} \left(1 - \frac{c}{L} \right) \quad (3)$$

where γ_{∞} is the friction coefficient measured in an infinite system, and c is a constant that depends on the array structure (simple cubic, BCC, FCC, ...). In our case, due to the periodic boundary conditions, the simple cubic array applies, yielding $c = 2.8373 a_t$ [15].

Based on this result, the full analysis of microrheology therefore requires

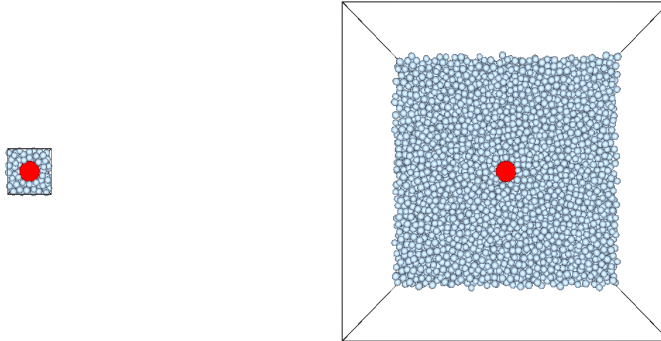


Figure 1: Snapshots of the systems with $N = 216$ and 32768 particles (left and right panels, respectively), with the same scale. The tracer, with $a_t/a = 3$, is marked in red, and the particles in front of it have been removed.

simulations of systems with different sizes, to extrapolate the friction coefficient γ_∞ using Eq. 3, for a single value of the force, volume fraction, or tracer size. Because the simulation time for a system of N particles evolves as $\sim N \ln N$, it is important to state the validity of this extrapolation, which is the main aim of the present work.

Previous simulations in passive microrheology, i.e. without external force acting on the tracer, have shown that Eq. 3 describes the dependence of the diffusion coefficient ($D_{\text{eff}} = k_B T / \gamma_{\text{eff}}$) on the system size [16, 17]. Evenmore, the value of γ_∞ , extracted from the fitting corresponds to the Stokes value, with slip boundary conditions and the viscosity calculated from Green-Kubo integration of the stress autocorrelation function [16]. We check here if those conclusions are valid for a finite force, helping in understanding the generalized Stokes-Einstein relation. The application of an external force implies a continuous input of energy in the system, needing an energy sink, where this energy is dissipated, which is an important difference with respect to previous works in passive microrheology. In our case, energy is dissipated in the friction with the solvent, given by γ_0 .

In order to test the theoretical model, we have run simulations of systems with $N = 216, 512, 1000, 2197, 4096, 8000, 15625$ and 32768 particles. Fig. 1 presents snapshots of the extreme sizes, with a tracer three times larger than the bath particles, $a_t = 3a$. In our simulations, lengths are measured in units of the mean bath particle radius, a , energy in units of the thermal energy $k_B T$, and mass in units of the particle mass, m . For the friction coefficient with the solvent, we take $\gamma_0 = 5 \sqrt{m k_B T} / a$, which gives a mean

single particle diffusion coefficient of $D_0 = k_B T / \gamma_0 = 0.2 a \sqrt{k_B T / m}$ for the bath particles. The volume fraction of the bath is $\phi = 0.50$. The external force is applied in the x -axis. The equations of motion are integrated using the Heun algorithm [37], with a time step of $\delta t = 0.0005 a \sqrt{m / k_B T}$. In this algorithm, the friction force is integrated analytically in the time interval δt .

3. Computational implementation

From a computational point of view, the problem requires a large set of simulations of tracer trajectories in systems of different sizes (N); therefore, the use of high performance computing is mandatory.

In the model it is possible to identify two parallelism levels. Level 1 allows us to accelerate the computation of a single tracer trajectory; and level 2 is related to the computation of several trajectories. To compute the function $\gamma_0 / \gamma_{\text{eff}}(a/L)$ it is necessary to analyze the tracer dynamic for different sizes of the bath. Therefore, the second level of parallelism can be exploited executing simulations with different number of particles in parallel, needed for the extrapolation leading to γ_∞ .

We have accelerated the computation of a single tracer trajectory (level 1) by means of GPU computing using CUDA interface [30, 31]. Our attention has been focused on the acceleration of the routines which evaluate the tracer dynamics; mainly, the calculation of interaction forces and integration of the equations of motion [32]. Every simulation of the tracer dynamic includes a massive parallelism since the same computation has to be completed for all particles in the bath. This parallelism is harnessed by the simulations computed on GPUs.

The whole set of simulations (level 2) to analyze the friction coefficient has been distributed on modern Multi-GPU clusters, which provide CPU-cores and GPUs which can compute several simulations in parallel. A subset of tracer trajectories can be computed in parallel on the CPU-cores and GPUs of a cluster. This way, every CPU-core (GPU) can execute the sequential code in Fortran (CUDA) to compute a single tracer trajectory, and the whole set of tasks can be run on the heterogeneous cluster with the collaboration of the CPU-cores and the GPUs. Moreover, the computational loads of the corresponding tasks are also different because the computation of trajectories in systems with different sizes are needed. Consequently, it is necessary to define an appropriated tasks scheduling to obtain the optimal parallel performance. Several strategies have been devised for this purpose, some of

them specifically for particle systems [33]. Here, we have adapted a genetic algorithm (GA) to optimize the trajectories scheduling.

There is a wide variety of previous work where genetic algorithms are used to solve scheduling problems [34]. GA works with a set of individuals which represent every possible solution of the scheduling policy problem (*population*). The procedure evolves iteratively starting with a random set of individuals, P_0 , and at every iteration, i , the selection and genetic operators are applied to the population, P_i . Thus, the population is constantly evolving. The selection mechanism allows that the individuals of new populations are closer to the optimal.

The methodology to execute the microrheology model with several system sizes on a Multi-GPU cluster includes the following stages:

1. Profiling stage, which estimates the sequential runtime of the microrheology model on every computational resource (GPU/ CPU-core) for the considered system sizes of the problem.
2. GA scheduling estimation, which plans the set of trajectories on every CPU-core and GPU to optimize the parallel runtime of all simulations by the GA. The inputs of this stage are: the profiling stage output, the number of computational resources of every type on the cluster (number of GPUs/ CPU-cores) and the number of trajectories of every system size of the model.
3. Parallel execution of the model on the cluster according to the scheduling estimation.

The software to carry out stages 2 and 3 has been implemented in Python and is freely available at <https://github.com/2forts/GENS>.

To analyze the friction coefficient, we study the set of simulations with sizes: $N = 216, 512, 1000, 2197, 4096, 8000, 15625$ and 32768 , with 500 trajectories of 500 time units (corresponding to 10^6 time steps). So, the model has to compute a total of 4000 trajectories. A state-of-the-art cluster has been considered as the test platform. It is composed by 4 nodes with a multiprocessor of 16 CPU-cores (Bullx R424-E3 Intel Xeon E5 2650 with 8GB RAM) and 2 GPUs NVIDIA Tesla M2070.

Table 1 shows the runtime on a CPU-core and a GPU to simulate a single trajectory on such test platform obtained in the profiling stage. The acceleration factors (AF) on GPU vs. CPU-core to simulate a single trajectory are also included. High acceleration factors, specially for large system sizes,

are obtained (up to $24\times$). However, for small problems the use of the GPU computing has no advantage.

From the profiling data, the scheduling is estimated by the GA according to the available resources on the cluster. If the 8 GPUs of the cluster and 56 CPU-cores are used (8 CPU-cores are devoted to controlling the 8 GPUs) to simulate the 4000 trajectories included in the model, the runtime is 202,4 hours when the GA scheduling is applied. If only a multiprocessor of a node was exploited, the runtime would be 2905 hours for all trajectories. To illustrate the advantages of the GA scheduling in terms of runtime for the analyzed model, Table 2 shows the runtime for the GA and a Round Robin approach for several configurations of the cluster and also the GA acceleration factor (GAAF). The results show that the GAAF ranges from $1,0\times$ (the homogeneous cluster configurations) to $2,7\times$ (the most heterogeneous cluster configuration). So the more heterogeneous the cluster is, the more advantages the GA reaches. Therefore, the use of a multi GPU-CPU cluster in combination with the GA scheduling have allowed that every simulation is executed on a CPU/GPU according to its size, reaching a considerably reduction of the total runtime of the microrheology model.

Table 1: Execution time (in seconds) of the simulation of a single trajectory for the eight sizes of the problem (N). t_{GPU} and t_{CPU} columns identify the runtime for a single trajectory on a GPU NVIDIA Tesla M2070/a and CPU-core Bullx R424-E3, respectively. AF is the acceleration factor of a GPU vs. a CPU-core for each N .

N	t_{GPU}	t_{CPU}	AF
216	1580	790	0.5
512	1785	1860	1.0
1000	2240	3715	1.7
2197	2930	8710	3.0
4096	4450	18065	4.1
8000	7650	43080	5.6
15625	12050	113940	9.5
32768	20012	479313	24.0

4. Results

The effective friction coefficient probed by a tracer of the same size as the bath particles develops a plateau for small driving forces, and decreases

Table 2: Parallel execution time, in hours, for a Round Robin placement (RR) and the GA solving 500 trajectories of 500 time units ($N = 216, 512, 1000, 2197, 4096, 8000$ and 15625) for the cases A) 14 CPU-cores and 2 GPUs; B) 28 CPU-cores and 4 GPUs; C) 28 CPU-cores and 8 GPUs; D) 56 CPU-cores and 8 GPUs; E) 8 GPUs and F) 64 CPU-cores. GAAF shows the GA acceleration factor.

	A	B	C	D	E	F
RR	844.8	422.4	369.6	211.2	290.4	211.2
GA	410.4	206.4	139.2	102.5	283.2	206.4
GAAF	2.1	2.0	2.7	2.1	1.0	1.0

for increasing forces [7], in analogy with the shear viscosity in bulk systems. We will focus here on the linear regime at small forces, with large tracers, which is expected to be closer to the model of Newtonian fluids used in the theoretical description. Thus, we study first the behaviour of γ_{eff} with the external force for a tracer three times larger than the bath particles, $a_t/a = 3$. Fig. 2 shows the results for two systems with different number of particles: $N = 2197$ and $N = 216$. Indeed, γ_{eff} depends strongly on the system size, as expected from the theoretical analysis discussed previously.

The effective friction coefficient shows the same qualitative behaviour for a large tracer as the previously reported for $a_t = a$ (a plateau at small forces, followed by a force-thinning regime), irrespective of the number of particles in the system. The linear regime at small forces extends to $F_{\text{ext}} \approx 10 k_B T/a$. Thus, we select a force of $F_{\text{ext}} = 2.5 k_B T/a$, which is well inside this linear regime. In the following, we first study finite size effects in different cases, and then compare with the theoretical model.

The first point we analyze is the volume occupied by the tracer. In the simulations shown in Fig. 2, the tracer is inserted in the system, compressing it, and increasing effectively the volume fraction of the bath. Note that the increase of volume fraction is larger for smaller systems. In the theoretical model, the properties of the bath are not affected by the insertion of the tracer, or by modifying the tracer lattice spacing, namely, the simulation box size. We have thus run simulations with different simulation boxes keeping the volume fraction of the system (bath and tracer) constant, and equal to 50% in all cases. The results are presented in Fig. 3, in comparison with the data from simulations without correcting the tracer volume. Both data sets agree for large systems, where the volume of the tracer is negligible, compared with the volume of the whole system, but differ significantly for

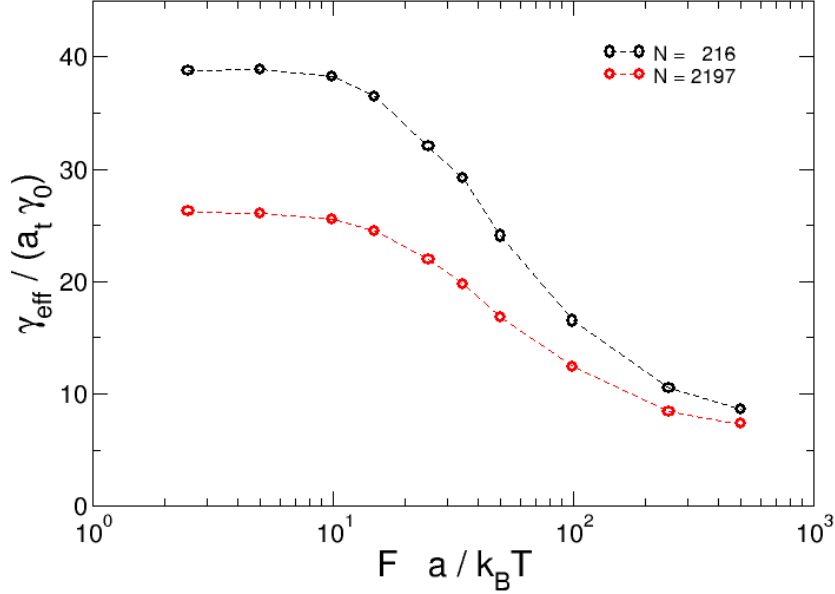


Figure 2: Effective friction coefficient for a system with $a_t/a = 3$, normalized with the friction with the solvent $a_t \gamma_0$. Two system sizes are considered, $N = 216$ and $N = 2197$, as labeled.

small systems. Notably, in this case, the friction coefficient is much larger when the tracer volume is not added to the system, due to the increase of effective volume fraction in the bath (note that the inverse friction coefficient is plotted in the figure).

In comparing with the theoretical prediction, we note that the simulation data for the system without the volume correction fits better to the expected qualitative behaviour for small systems (namely, a decreasing linear trend of $1/\gamma_{\text{eff}}$ vs. $1/L$). However, the results from the theoretical model are more strict than a linear dependence of $1/\gamma_{\text{eff}}$ vs. $1/L$; eq. 3 implies a relation between the slope and intercept. The thick dashed line in Fig. 3 shows the theoretical prediction (γ_∞ is fitted), for small and intermediate systems. The fitting is not satisfactory, probably due to the important differences between the simulated system and the theoretical model (continuous bath vs. particles, Newtonian fluid vs. viscoelastic bath, boundary condition in

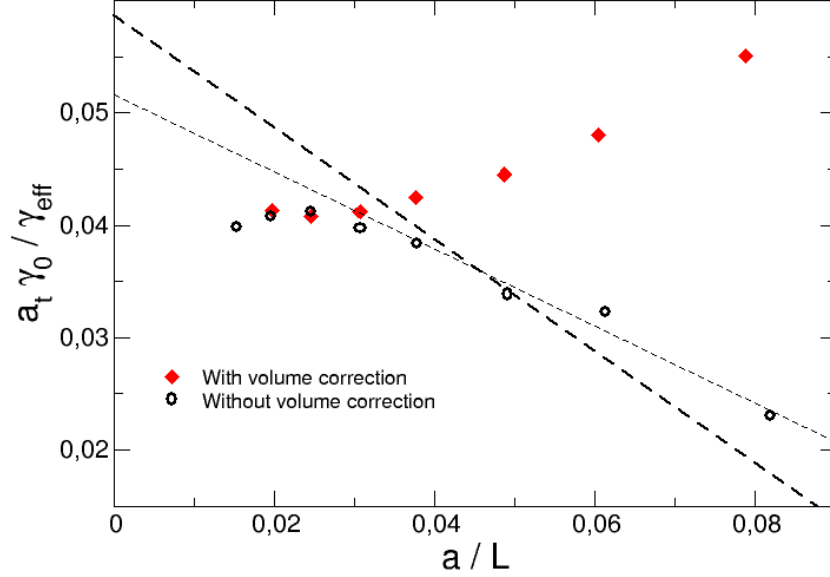


Figure 3: Effect of considering the volume of the tracer: normalized effective friction coefficient for a system with $a_t/a = 3$ as a function of the inverse system size, for a system with volume correction, or without it, as labeled. The thick dashed line is a free linear fitting to the data without volume correction, for systems up to $N = 8000$ particles, and the thick line is the fitting according to the theoretical model, Eq. 3.

the tracer surface...).

It must be mentioned that these deviations were not observed in passive microrheology [16, 17] (recall that Newtonian dynamics were used those simulations and no force was applied). In our case, however, the agreement with the theory is not quantitative. Still, a decreasing linear dependence is found for $1/\gamma_{\text{eff}}$ vs. $1/L$ (thin dashed line) although for large systems the data deviate from the linear trend.

The effect of fixing the center of mass (CM) of the system, or leaving it free is studied next. The application of an external force, even though applied onto a single particle, implies a displacement of the CM, while in a macroscopic system, this should be fixed. The CM can be fixed in the simulations artificially, correcting the particle positions at every time step.

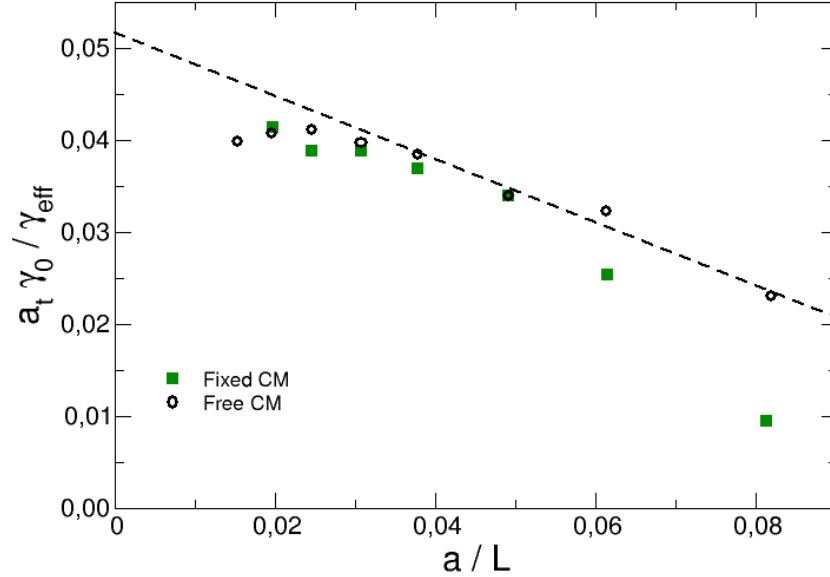


Figure 4: Effect of fixing the center of mass of the system in microrheology: normalized inverse effective friction coefficient as a function of the inverse system size, for a system with the CM fixed or free, as labeled. The dashed line is a linear fitting to the data for small and intermediate systems.

Again, this aspect is absent in the theoretical model, where the solvent is an incompressible Newtonian fluid. Fig. 4 presents the results of γ_{eff} for different system sizes from simulations with the CM fixed, in comparison with the results leaving it free (in both cases the tracer volume has not been considered in the total volume of the system).

The results for both cases differ for small sizes, but agree for large systems, when the effect of pulling a single particle becomes negligible, and thus the correction of the particle motion is less important. The data with the CM fixed deviate from a linear trend at both small and large systems, while the data for the free CM follows the linear trend, as shown above. Thus the following simulations are run with the CM free, to improve the comparison with the theory.

The microscopic motion of the particles is also affected by the solvent

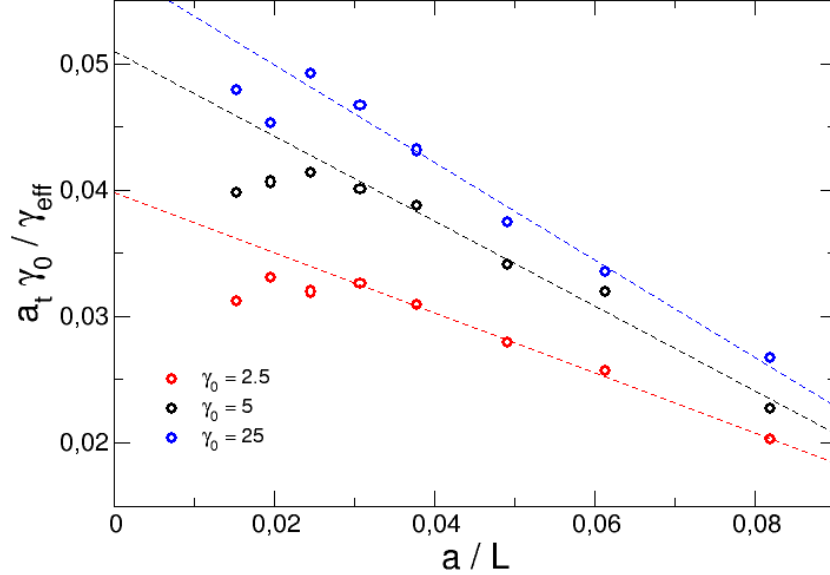


Figure 5: Effect of the solvent friction coefficient γ_0 on the effective friction coefficient. The lines show the linear fittings (dashed lines).

friction coefficient, $\gamma_i = \gamma_0 a_i$ – large values of γ_0 reduce the effect of inertia, making the dynamics more Brownian like. Again, the theoretical model does not consider explicitly this aspect; the bath in the theory is a continuous medium and not Brownian. Fig. 5 presents the results of simulations with different values of γ_0 . Upon increasing the friction with the solvent, $\gamma_{\text{eff}}/\gamma_0$ decreases, as the contribution from the solvent to the total friction experienced by the tracer increases. On the other hand, in all cases, the inverse friction coefficient shows a linear dependence on $1/L$ for not-too-large systems, as shown by the thin dashed lines.

Finally, we study the effect of the tracer size, as the assumption of a continuous bath is expected to be applicable if the tracer is much larger than the bath particles. Fig. 6 presents the results of the inverse effective friction coefficient as a function of the inverse system size for $a_t/a = 3$ and $a_t/a = 4$. In both cases, the CM is free, the volume of the tracer has not been considered, and $\gamma_0 = 5 \sqrt{mk_B T}/a$. The results show the same trend

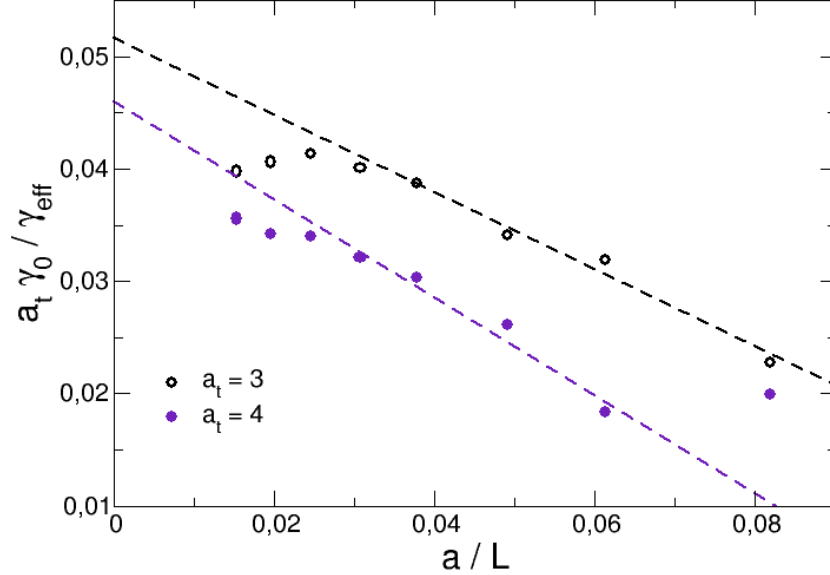


Figure 6: Effect of varying the tracer size, as labeled. The dashed lines show again the linear fittings to the data from small and intermediate systems.

for both sets of data; namely, a linear trend appears for small systems (thin dashed lines), while both of them deviate for large systems. The figure also allows checking if γ_{eff} is linear with the tracer size, as expected from Stokes' law. The results, however, indicate that the friction coefficient grows with a_t faster than linear, indicating that the Stokes' regime is not valid in this system and for this range of tracer sizes.

The analysis presented so far have shown that the theoretical prediction is only qualitatively followed for small and intermediate systems, with the appropriate conditions in the simulations, but fails for large systems in all cases. Thus, we analyze in the following the reason for this discrepancy.

Within the theoretical model, the friction experienced by the tracer is calculated from the velocity profile in the bath [38]. Therefore, we study the velocity of the bath particles in the simulations and compare it with the theoretical result. Because for large systems γ_{eff} becomes independent on the system size, we focus on the system with $N = 15625$ particles and

compare the velocity map with the theoretical results for a single particle in an incompressible Newtonian fluid. The latter is given, in polar coordinates, by [38]:

$$v_r(r, \theta) = u_{\text{tracer}} \cos \theta \left(\frac{3a_t}{2r} - \frac{a_t^3}{2r^3} \right) \quad (4)$$

$$v_\theta(r, \theta) = -u_{\text{tracer}} \sin \theta \left(\frac{3a_t}{4r} + \frac{a_t^3}{4r^3} \right) \quad (5)$$

where θ is the angular coordinate, measured from the force direction, and u_{tracer} is the tracer velocity. This result is valid for low Reynolds number, which is indeed our case; a rough estimate of the ratio of inertia to viscous forces is $(mu_{\text{tracer}}/a_t)/(\gamma a_t)$ which is below 0.1 in all cases.

Fig. 7 shows both components of the velocity in the bath (divided by the tracer velocity) from simulations (left panels) and theory (right ones). In the simulations, the system with $N = 15625$ has been run for ca. $5 \cdot 10^4$ time units (amounting to 10^8 integration steps), to improve the statistics. The comparison shows some important differences, and some similarities. The normal component shows that the velocity in front of the tracer is positive in both the simulations and theory, and negative behind it; however while it decays monotonously to zero from the tracer to infinity in the theory, panel (c), in the simulations, it oscillates – panel (a). Transversal to the force, the velocity has a negligible normal component both in the simulations and in the theory.

The angular component (bottom panels), on the other hand, shows also some differences between the simulations and the theory. In the model, panel (d), the minimum is in the tracer surface, perpendicular to the force direction (recall that stick boundary conditions are assumed in the tracer surface), and decays monotonously to zero. The simulations, shown in panel (b), are much noisier, but a dip develops in this region; further from the tracer (in the direction perpendicular to the force), v_θ becomes positive (but small) and decays to zero far from the tracer. In this case, oscillations are not observed, probably due to the poor statistics.

The radial component is studied in more detail in Fig. 8, where the bath velocity in front of the tracer is studied (to reduce the statistical noise, it has been averaged over an angle of 30°). The oscillations of the bath velocity have a wavelength of one (bath) particle diameter, and reproduce the oscillations of the density profile (black line). Thus, these are a direct consequence of

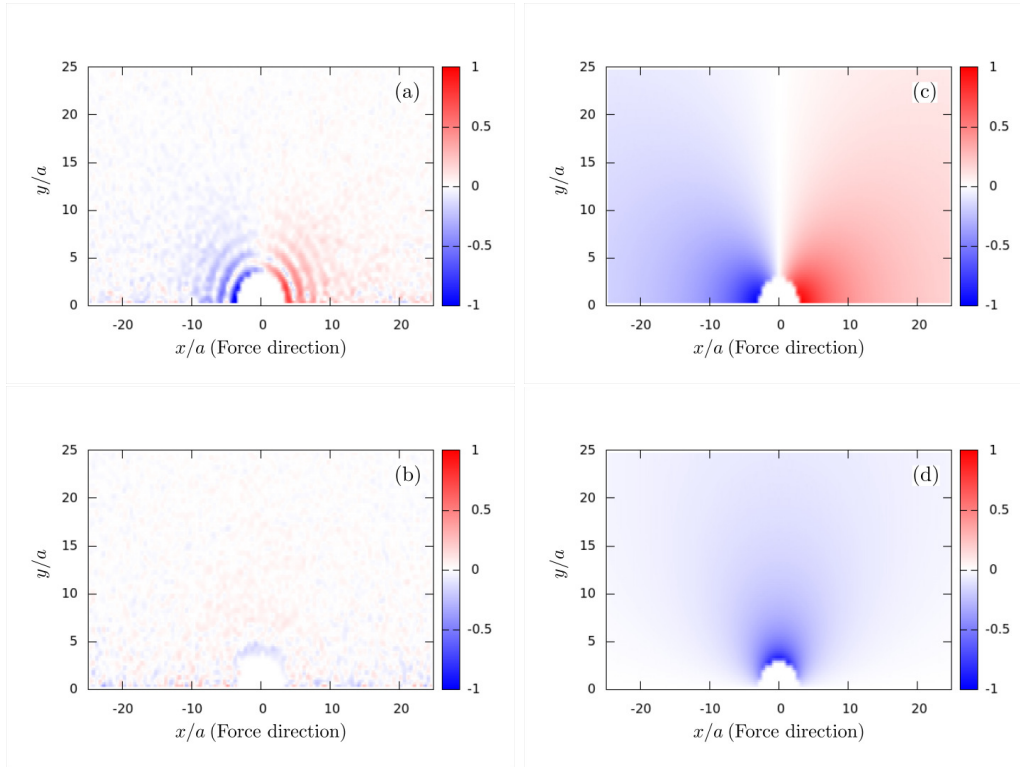


Figure 7: Velocity maps in the bath from simulations (panels (a) and (b)) and theory (panels (c) and (d)); the radial (angular) component is presented in the top (bottom) panels.

the finite size of the bath particles. The inset to this figure presents the same data on a logarithmic scale, showing that the bath velocity in front of the particle decays faster in the simulations than in the theory, probably due to the friction with the solvent and the Brownian motion that disrupt the transfer of momentum in the bath. Notably, the velocity in the bath is negligible, within the noise level, for distances of ca. $20 - 25a$. The systems with a box size smaller than (twice) this value should present *interactions* between the tracer and its periodic images due to the cutoff of the velocity profile. In systems with a large simulation box, the velocity profile can decay inside the box, and the friction experienced by the tracer is not affected by its periodic images. It can be concluded, therefore, that large systems, beyond this limit, should be free of finite size effects, and the limit corresponds to the systems of 8000 particles, as indeed observed in the evolution of γ_{eff} vs.

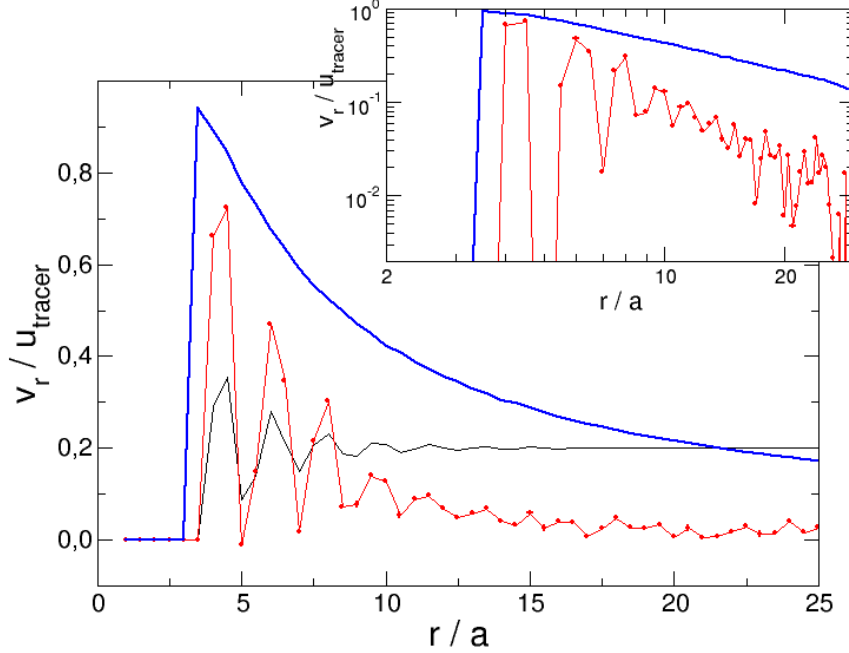


Figure 8: Normalized radial component of the bath velocity in front of the tracer, from simulations (red points and lines) and theory (thick blue line). The bath density is also presented (thin black line), scaled. The inset shows the same velocity data in logarithmic scale.

L , studied previously.

5. Conclusions

We have presented simulations of active microrheology in hard colloids. This system is strongly affected by finite size effects, which have been analyzed using a model developed previously for an array of tracers moving in a Newtonian fluid. According to the model, the inverse effective friction felt by the tracer depends linearly on the inverse lattice parameter. In order to test this prediction, different simulation conditions have been proposed (consideration of the tracer volume, motion of the center of mass, tracer size, and friction with the solvent), but deviations for large systems are observed in all cases, although linear trends have been observed in particular cases for small and intermediate systems.

The deviations of γ_{eff} with respect to the theoretical behaviour indicate that the approximations in the theoretical model are too strong for the simulated system. This invalidates the use of this model to extract the effective friction coefficient for a macroscopic system from the linear extrapolation $1/L \rightarrow 0$. Previous simulations of passive microrheology in a bath of particles undergoing molecular dynamics did follow the linear trend, and could use it to extract γ_{∞} and check Stokes' law. The failure of the model in our case must be attributed to the different microscopic dynamics, which is dissipative in our case. This, presumably, implies a damping for the shear waves, and a saturation of the finite size effect predicted by the theory.

Computationally, on the other hand, it presents an important advantage; namely, simulations in a large enough system can be used to obtain the effective friction coefficient probed by a tracer, skipping the necessity of making simulations with different system sizes and rely on an extrapolation to $1/L \rightarrow 0$. It must be mentioned, however, that the minimum size of the system to avoid finite size effects may depend on the tracer size.

The results presented here concern a system of quasi-hard spheres, i.e. with short-range interactions. While it is difficult to extrapolate these results for systems with interactions of longer range, structural correlations will extend to larger distances, possibly increasing the range of validity of the continuous medium approximation for the bath. However, if the microscopic dynamics is indeed responsible for the damping of the shear waves and hydrodynamic correlations, as proposed here, it should eventually dominate over long enough distances, making a proper analysis of finite size effects mandatory. The technique proposed here (GA scheduling of simulation tasks of different loads) is a powerful tool for this analysis.

Acknowledgments

This work has been supported by the Spanish Science and Technology Commission (CICYT) under contracts TIN2015-66680 and FIS2015-69022-P; Junta de Andalucía under contract P12-TIC-301 in part financed by the European Regional Development Fund (ERDF). G. Ortega is a fellow of the Spanish 'Juan de la Cierva Incorporación' program.

References

- [1] P.M. Chaikin, T.C. Lubensky, Principles of Condensed Matter Physics, Cambridge University Press, Cambridge (UK), 1995.

- [2] Ed. A. Fernandez-Nieves, A.M. Puertas, *Fluids, Colloids and Soft Materials*, John Wiley & sons, New Jersey (USA), 2016.
- [3] R. Khare, D.S. Devarajan, Molecular simulations of nanocolloids, *Curr. Op. in Chem. Engineering*, **16**, 86 (2017).
- [4] R.G. Larson, *The structure and rheology of complex fluids*, Oxford University Press, USA, 1999.
- [5] P. Cicuta, A.M. Donald, Microrheology: a review of the method and applications, *Soft Matter* **3**, 1449–1455 (2007).
- [6] L. Wilson, W. C. K. Poon, Small-world rheology: an introduction to probe-based active microrheology, *Phys. Chem. Chem. Phys.* **13**, 10617–10630 (2011).
- [7] A.M. Puertas, Th. Voigtmann, Microrheology of colloidal systems, *J. Phys.: Condens. Matter* **26**, 243101 (2014).
- [8] E. Furst, T. Squires, *Microrheology*, Oxford University Press, UK, 2017.
- [9] T.G. Mason, D.A. Weitz, Optical Measurements of Frequency-Dependent Linear Viscoelastic Moduli of Complex Fluids, *Phys. Rev. Lett.* **74**, 1250 (1995).
- [10] T.G. Mason, H. Gang, D.A. Weitz, Rheology of complex fluids measured by dynamic light scattering, *J. Molec. Structure* **383**, 81–90 (1996).
- [11] M. Umansky, D. Weihs, Novel algorithm and MATLAB-based program for automated power law analysis of single particle, time-dependent mean-square displacement, *Comp. Phys. Comm.* **183**, 1783–1792 (2012).
- [12] H.-H. Jeong, A.G. Mark, T.-C. Lee, M. Alarco-Correa, S. Eslami, T. Qiu, J.G. Gibbs, P. Fischer, Active Nanorheology with Plasmonics, *Nano Letters* **16**, 4887–4894 (2016).
- [13] T. M. Squires, Nonlinear Microrheology: Bulk Stresses versus Direct Interactions, *Langmuir* **24**, 1147–1159 (2008).
- [14] T.M. Squires, T.G. Mason, *Fluid Mechanics of Microrheology*, *Annu. Rev. Fluid Mech.* **42**, 413 (2010).

- [15] H. Hasimoto, On the periodic fundamental solutions of the Stokes equations and their application to viscous flow past a cubic array of spheres, 1959, *J. Fluid Mech.* **5**, 317–328.
- [16] I.-C. Yeh, G. Hummer, System-Size Dependence of Diffusion Coefficients and Viscosities from Molecular Dynamics Simulations with Periodic Boundary Conditions, *J. Phys. Chem. B* **108**, 15873–15879 (2004).
- [17] R.O. Sokolovskii, M. Thachuk, G N. Patey, Tracer diffusion in hard sphere fluids from molecular to hydrodynamic regimes, *J. Chem. Phys.* **125**, 204502 (2006).
- [18] F. Ould-Kaddour, D. Levesque, Molecular-dynamics investigation of tracer diffusion in a simple liquid: Test of the Stokes-Einstein law, *Phys. Rev. E* **63**, 011205 (2000).
- [19] J.R. Schmidt, J.L. Skinner, Hydrodynamic boundary conditions, the Stokes-Einstein law, and long-time tails in the Brownian limit, *J. Chem. Phys.* **119**, 8062–8068 (2003).
- [20] H.K. Shin, C. Kim, P. Talkner, E.K. Lee, Brownian motion from molecular dynamics, *Chem. Phys.* **375**, 316–326 (2010).
- [21] I.C. Carpen, J.F. Brady, Microrheology of colloidal dispersions by Brownian dynamics simulations, *J. Rheol.* **49**, 1483–1502 (2005).
- [22] I. Gazuz, A.M. Puertas, Th. Voigtmann, M. Fuchs, Active and Nonlinear Microrheology in Dense Colloidal Suspensions, *Phys. Rev. Lett.* **102**, 248302 (2009).
- [23] C.J. Olson Reichhardt, C. Reichhardt, Fluctuations, jamming, and yielding for a driven probe particle in disordered disk assemblies, *Phys. Rev. E* **82**, 051306 (2010).
- [24] M.V. Gnann, I. Gazuz, A.M. Puertas, M. Fuchs, Th. Voigtmann, Schematic models for active nonlinear microrheology, *Soft Matter* **7** 1390 (2011).
- [25] Ch.J. Harrer, D. Winter, J. Horbach, M. Fuchs, Th. Voigtmann, Force-induced diffusion in microrheology, *J. Phys: Condens. Matter* **24**, 464105 (2012).

- [26] D. Winter, J. Horbach, P. Virnau, K. Binder, Active Nonlinear Microrheology in a Glass-Forming Yukawa Fluid, *Phys. Rev. Lett.* **108**, 028303 (2012).
- [27] C.F.E. Schroer, A. Heuer, Anomalous diffusion of driven particles in supercooled liquids, *Phys. Rev. Lett.* **110**, 067801 (2013).
- [28] D. Winter, J. Horbach, Nonlinear active micro-rheology in a glass-forming soft-sphere mixture, *J. Chem. Phys.* **138**, 12A512 (2013).
- [29] T. M. Squires, J. F. Brady, A simple paradigm for active and nonlinear microrheology, *Phys. Fluids*, **17**, 073101 (2005).
- [30] G. Ortega, A.M. Puertas, E.M. Garzón, Accelerating the problem of microrheology in colloidal systems on a GPU, *J. Supercomput* **73**, 370–383 (2017).
- [31] G. Ortega, A.M. Puertas, F.J. de Las Nieves, E.M. Garzón, GPU Computing to Speed-Up the resolution of microrheology models, *Algorithms and Architectures for Parallel Processing: 16th ICA3PP*, Granada, Spain, Springer International Publishing, Cham, pp. 457–466, (2016).
- [32] I.V. Morozov, A.M. Kazennov, R.G. Bystryi, G.E. Norman, V.V. Pisarev, V.V. Stegailov, Molecular dynamics simulations of the relaxation processes in the condensed matter on GPUs, *Comp. Phys. Comm.* **182**, 1974–1978 (2011).
- [33] W.M. Brown, P. Wang, S.J. Plimpton, A.N. Tharrington, Implementing molecular dynamics on hybrid high performance computers - short range forces, *Comp. Phys. Comm.* **182**, 898–911 (2011).
- [34] V. Sels, J. Coelho, A. Dias, M. Vanhoucke, Hybrid tabu search and a truncated branch-and-bound for the unrelated parallel machine scheduling problem, *Computers & Operations Research* **53** 107– 117, (2015).
- [35] J.K.G. Dhont, *An Introduction to Dynamics of Colloids*, Elsevier, Amsterdam (Holland) 1996.
- [36] E. Lange, J.B. Caballero, A.M. Puertas, M. Fuchs, Comparison of structure and transport properties of concentrated hard and soft sphere fluids, *J. Chem. Phys.* **130**, 174903 (2009).

- [37] W. Paul, D.Y. Yoon, Stochastic phase space dynamics with constraints for molecular systems, *Phys. Rev. E* **52**, 2076 (1995).
- [38] E. Guyon, J.P. Hulin, L. Petit, C.D. Matescu, *Physical Hydrodynamics*, Oxford University Press, Oxford (UK), 2001.